RESEARCH ARTICLE

Macromolecular Materials and Engineering
www.mame-journal.de

Freeform Fabrication of Pneumatic Soft Robots via Multi-Material Jointed Direct Ink Writing

Zhenhua Wang, Boyu Zhang, Weicheng Cui, and Nanjia Zhou**

Pneumatically actuated soft robots have attracted significant attention in recent years due to their non-linear structures for performing biomimetic motions to enhance human-machine interactions. However, manufacturing soft robots, especially those featuring complex 3D structures, still faces significant challenges as traditional lithography-based micro/nanofabrication technologies have some limitations, such as limited material choices and layer-by-layer architectures. In this work, a facile multi-material jointed direct ink writing (MJDIW) printing method is introduced. In comparing with the traditional micro/nanofabrication and other additive manufacturing methods, the method enables truly freeform 3D printing to fabricate entirely soft actuators and robots with complex 3D structures, while integrating materials with different mechanical characteristics to expand the manufacturing capabilities of additive manufacturing methods. The material properties and printing parameters, and conducted finite element analysis (FEA) is systematically investigated to provide the general design guidelines through simulating actuator motions. Several actuators such as linear elongation and bending actuators are manufactured either by employing a single material or multiple materials with different mechanical properties. Finally, a multi-directional soft manipulator with complex internal channels is printed using different materials to illustrate the versatility of the printing methods.

1. Introduction

Soft robots are viewed as potential replacement of their rigid counterparts to perform compliant and delicate manipulations including soft grasping,[1] underwater sampling,[2] and medical surgery.[3] Among different types of soft robots, pneumatic ones are used most widely because of their simple design, cost-effectiveness and large output force. Pneumatic soft robots are composed of different functional materials featuring a variety of electrical, optical, and mechanical properties to increase their intelligence and automation. For example, materials with tunable elastic moduli ensure the stiffness gradient in the structure.[4] Electrical and optical functional materials have also been integrated for somatosensitive sensing of soft robots.[5,6] Recently, several stimuli-response materials have also been embedded into or coated on the soft robots to mimic certain biological behaviors, including perspiration,[7] camouflage,[8] etc.

Conventional casting methods such as pin casting,[9] lost wax casting[9] and rotational molding,[10] as well as emerging methods such as soft lithography,[11] all have difficulties in the manufacturing of complex 3D structures. The completion of internal channels also relies on multiple adhesion steps which may cause delamination upon channel inflation.[12] Therefore, the fabrication of the soft bodies with complicated internal structure and different materials has become a great challenge.

As additive manufacturing (also known as 3D printing) technologies develop in recent years, various printing methods have been used to fabricate soft pneumatic actuators and robots. Among them, fused deposition modeling (FDM) has been used to print soft grippers and actuators.[13] However, it suffers from limited material choices, i.e., thermoplastic materials only, such as thermoplastic polyurethane (TPU) (Shore hardness of 60–90 A), which is too stiff for the soft robots. Stereolithography (SLA) technology has also been employed to print soft actuators. However, again due to the generally stiff materials and relatively low ultimate strain, the printed actuators feature limited motions. Besides, SLA method requires an additional cleaning step to remove uncured resins from the inner chambers which is often challenging.[14] Recently, a soft gripper using highly stretchable and UV curable elastomer was reported.[15] Compared to the commercially available silicone-based materials, it suffers from

Z. Wang
Zhejiang University-Westlake University Joint Training
Zhejiang University
866 Yuhangtang Road, Hangzhou, Zhejiang Province 310058, China
B. Zhang, N. Zhou
Key Laboratory of 3D Micro/nano Fabrication and Characterization of Zhejiang Province
School of Engineering
Westlake University
18 Shilongshan Road, Hangzhou, Zhejiang Province 310024, China
E-mail: zhounanjia@westlake.edu.cn
W. Cui
Key Laboratory of Coastal Environment and Resources of Zhejiang Province
School of Engineering
Westlake University
18 Shilongshan Road, Hangzhou, Zhejiang Province 310024, China
E-mail: cuiweicheng@westlake.edu.cn

The ORCID identification number(s) for the author(s) of this article can be found under https://doi.org/10.1002/mame.202100813

DOI: 10.1002/mame.202100813

low elastic modulus and low tensile elongation at break. Selective Laser Sintering (SLS) can also be used to print soft grippers with TPU powder, yet the possible wall thickness (1–10 mm) and channel sizes (>10 mm) using SLS are limited.[16]

Silicone rubbers (elastic moduli<1 Mpa) are widely used in casting method to design and fabricate soft robots.[17] Low viscosity (several Pa s) before curing and long cure time (about 2–10 h) present challenges for FDM and SLS. Commercially available silicone-based flexible SLA and Polyjet materials typically have a relatively low elongation yield (≈200%),[18] while silicone rubbers with the same hardness elongate up to ≈400%.[19] Direct ink writing (DIW) technology is viewed as the potential solution due to its versatile material compatibility, accessibility, and ability to heterogeneously integrate multiple materials into programmed 3D architectures.[20] Plott et al.[19] successfully printed pneumatic bending actuators using DIW method. The suspended structures must be designed with small gaps as the silicone inks cannot sustain their own shapes when the gaps become wider(>10 mm). Yirmibesoglu et al.[12] printed silicone rubber onto a heating stage with a temperature of 80 °C to accelerate the curing process which helped the printed structures to maintain their shapes. However, this method is not applicable to the silicone rubber with high curing temperatures and long curing time. Schaffner et al.[21] printed different actuators with silicone rubbers of different elastic moduli via multimaterial DIW. A fugitive ink (carrageenan) was used to print inner channels with resolutions of ≈1 mm. Yet printing speed became an issue due to the printing of fugitive part. To print silicone rubber-based structures with complicated inner channels, embedded DIW (EDIW) was proposed. Several attempts were made to print them within the support matrix, including carbomer,[22] silicone oil,[20] hydrogels.[23] Tubes,[24] woodpile[23] or other lattice geometries,[25] model octopus and jellyfish[22] and other structures were successfully printed. The matrix materials can be either curable or removable. The former strategy integrated the matrix material as part of the main body which cured together with the printed filaments.[5] For example, a sacrificial and a conductive sensor material were printed into the silicone rubber matrix which was cast in a mold to fabricate soft fingers. However, the external shapes were limited by the mold structures. Recently, Sparrman et al.[26] printed a bellow-based soft linear actuator and a manipulator in the Carbomer gel using silicone. This work proved the practicability of freeform printing of pneumatic actuator. However, a single material was used to print soft actuators in their work, which is insufficient for most pneumatic actuators. For example, the widely used bending actuator (PneuNet actuator) needs an extensible top layer and inextensible, but flexible, bottom layer.[11] The stiffness distribution of top layer can also be programmed for conformal operation and bio-inspired motions.[27] For soft robots suitable of accomplishing complex tasks, soft manipulators integrating both arms and grippers are often fabricated employing materials with different stiffness.[28]

In summary, soft actuators using FDM, SLA, and SLS methods are mainly challenged by the limited choices of materials and capabilities in manufacturing complex 3D structures. On the other hand, traditional DIW method, despite its expanded material compatibility, also face difficulties in printing complex pneumatic structures with inner channels. Jointed DIW feature freeform 3D printing which is ideal for manufacturing soft robots featuring complex geometries. Together with multimaterial printability, our multimaterial jointed DIW method allow the digital programming of functional materials into truly 3D architectures.

In this work, we propose a multi-material jointed DIW (MJDIW). The printing parameters are explored to provide the general guidelines for printing soft actuators and robots. Various actuators and a soft manipulator with complicated inner structures are printed using MJDIW method to demonstrate the versatility of our method. Lastly, we demonstrate a printed manipulator capable of finishing a delicate shaft and hole mating task.

2. Experimental Section

2.1. Printing Method and Hardware

There are four steps of the MJDIW method (**Figure 1**a): 1) Preparing the matrix. To accomplish embedded printing, the matrix must be a shear-thinning yield stress fluid. It must have suitable storage modulus and yield stress to ensure the support of the printed structures and the free travel of the translating nozzles. 2) Printing single or multi-materials in the matrix and curing the structure after printing (Figure 1b, Video S1: Supporting Information); 3) Liquefying the matrix to release the cured structures; 4) Cleaning the remaining matrix and attaching the air tube. A monolithically printed soft manipulator is shown in Figure 1c.

The printing process is finished using a custom-made 3-axis 3D printer. The ink is housed in a syringe (10 mL, EFD inc.) attached by a Luer-lock to a commercial nozzle (inner diameter, ID = 650 μm, Nordson EFD). The printing path is generated via the production of G-code that outputs the XYZ motion of a custom-made 3D printer. G-code is generated either by hand or using commercial software. The work uses the pressured air regulated by fluid dispenser (Ultimus V, EFD Inc) to extrude the ink. The extrusion speed is controlled by the pressure. The exploration of printing parameters is shown in Supporting Information (Figure S1, Supporting Information). The printing parameters are listed in Table S1 (Supporting Information).

2.2. Ink Formulation

The supporting bath is prepared by dissolving 0.3% w/w carbomer ETD 2020 (Lubrizol) in deionized water, then 10 M NaOH is added to neutralize the solution and form the carbomer gel. After degassed in the vacuum, the gel is ready for printing.

The soft ink is prepared by mixing part A and B of Dragon Skin 10 with 0.3%w/w Slo-Jo as the curing retarder and 1.5%w/w Thieve as the thicker (with respect to part A, all from smooth on). The intermediate ink is prepared by mixing part A and part B of Dragon skin 30 with 3% w/w Slo-Jo and 1.5% w/w (with respect to part A, all from smooth on). The hard ink is prepared by mixing SE1700 (Dow Corning) and Sylgard 184 (Dow Corning) in the ratio of 2:1 and adding 10%w/w curing agent with respect to part A, respectively. All inks are mixed by a planetary mixer (ARE-310, Thinky Mixer) and then filled into a syringe.

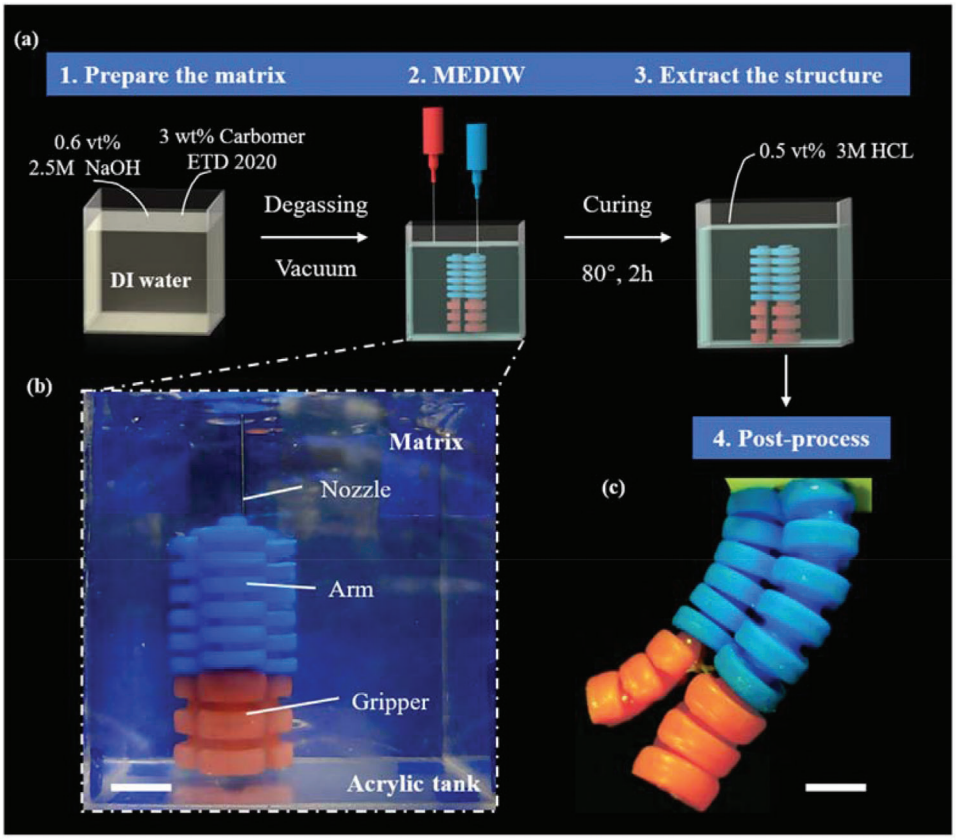

Figure 1. Fabrication of soft robots via MJDIW: a) Our printing method includes four steps: (1) matrix preparation: (2) printing; (3) releasing the structure; (4) post-processing; b) The printed soft manipulator consists of a soft arm and a soft gripper. The arm is printed by the hard ink (blue), whereas the gripper is printed by a relatively soft material (red) (Scale bar: 1 cm). c) The printed soft manipulator with the grippers open (Scale bar: 1 cm).

2.3. Material Characterizations

The rheological properties of the inks are investigated using a controlled stress rheometer (Discovery HR 10, TA Instrument Co., Ltd). Ink viscosities are measured as a function of shear rate from 0.01 to 10 000 s^{-1}. Storage and loss moduli are measured as a function of stress amplitude in the range of 0.1 to 500 Pa at a frequency of 1 Hz. The HB model regression of the matrix is performed using software (TRIOS). Dog-bone-shaped tensile test samples (ISO 527-5A) are fabricated. Tensile properties are measured by a universal mechanical testing equipment (CTM 6000, Xieqiang Instrument Manufacturing Shanghai Co., Ltd.).

2.4. FEA Simulation

The model of the actuators is first built in Solidworks 2019 (Dassault), and then exported as the .igs file to be imported into Abaqus 6.14 (Dassault). The sizes of the printed actuators are shown in Figure S7 (Supporting Information). The hyperelasticity of the material is described by Ogden 1st model based on the uniaxial tensile test. The pressure is exerted on the inner walls of the actuator, and a Encastre constraint is enforced on one end of the actuator (Figure S8, Supporting Information). The actuator is meshed by the 10-node quadratic tetrahedron hybrid element type (C3D10H).

3. Results and Discussion

3.1. Properties of the Matrix and the Ink

The matrix with suitable rheological properties and printing parameters are essential for MJDIW. In our research, the rheological properties of the matrix and silicone ink are first studied. ≈0.1, ≈0.3, ≈0.5, and ≈0.7%w/w Carbomer are dissolved in DI water, whose storage and loss moduli are compared to select the proper matrix. As shown in **Figure 2**a, the storage modulus increases with the increase of carbomer concentration. The yield stress of the matrix (the abscissa value of cross point of storage and loss moduli) also rises. To further identify the rheological properties, continuous shear flow tests are also conducted. From the Herschel–Bulkley (HB) model regression results for each matrix material (Figure 2b), τ_y (the yield stress), K (the consistency index), and n (the flow index) can be obtained. The Oldroyd number (Od number) is the most useful parameter to characterize the dimensions of the yielded areas of the HB fluids flowing around the printing nozzles, which can be calculated from the HB parameters and printing settings.[29] The HB parameters, printing

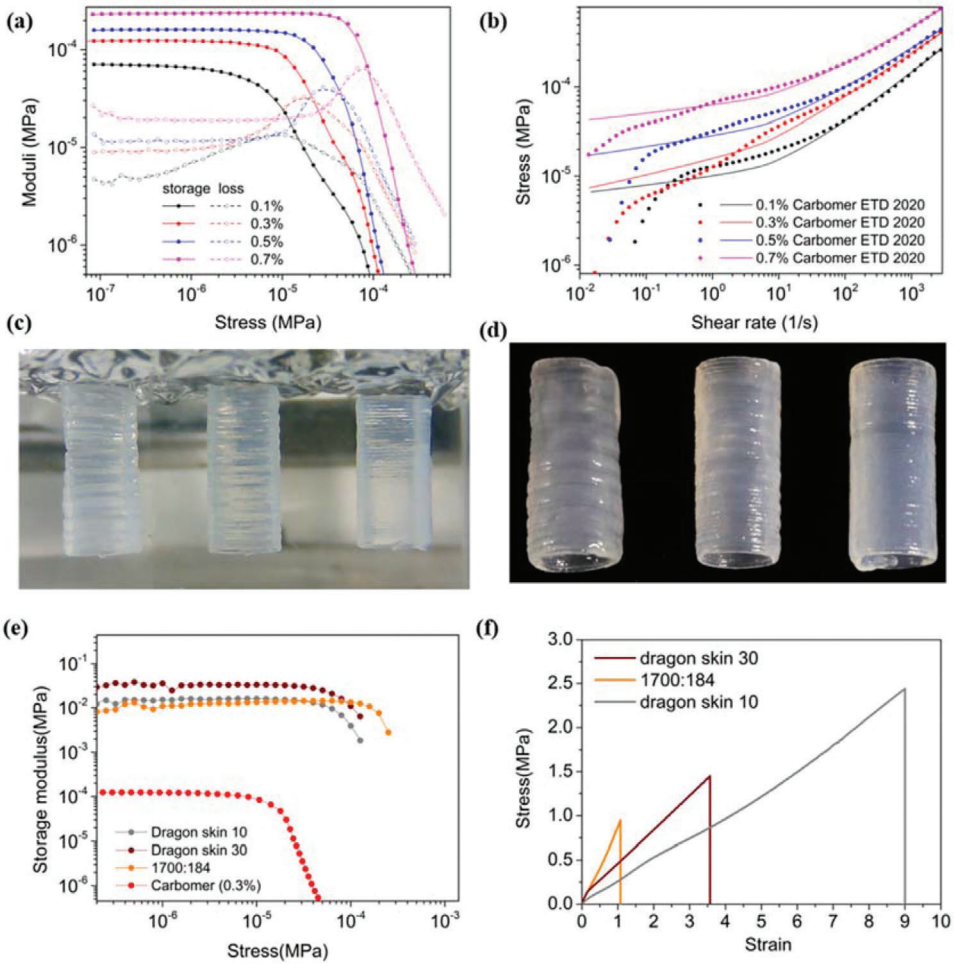

Figure 2. Rheological and mechanical properties of the matrix and ink: a) Storage and loss moduli versus stress curves of the matrix with 0.1, 0.3, 0.5, and 0.7%w/w of carbomer; b) Shear stress versus shear rate curves of the matrix. The data is fitted to the Herschel-Bulkley model. c) Three inks with different storage moduli are used to print thin wall structures. They are prepared by different ratios of Dow 1700 and Sylgard 184. From left to right, the ratios are 3:7, 5:5 and 7:3, respectively. As the concentration of 1700 increases, the storage modulus increases, and the wall becomes smoother. d) The cured thin wall structure; e) Storage modulus comparison with the matrix and the inks. f) Tensile measurement of the modified dragon skin 10, dragon 30 and 1700:184.

settings and Od numbers are listed in Table S2 (Supporting Information). The yield stress increases as the concentration of carbomer increases, which agrees well with the results in Figure 2a. The matrix with yield stress of ≈2.3 Pa (≈0.1%w/w) is unable to support the printed structure, whereas the matrixes with yield stress more than ≈30 Pa (≈0.5 and ≈0.7%w/v) are difficult to recover after the nozzle passes. Therefore, in our work, we choose ≈0.3%w/v carbomer gel as the matrix with the Od number of ≈0.4, which is close to the value in a previous report.[29]

Another challenge of the MJDIW approach is to print stacked filaments with sufficient fusion to guarantee the air-tightness of the chambers. When using inks with the moduli lower or equal to the matrix, unsuccessful fusion happens because of the following two reasons: 1) Inks with low storage moduli always have low yield stress. They are extruded by relatively low pressure, making them difficult to push away the matrix; 2) Low storage moduli result in insufficient ink fidelity and thus the printed filaments may be pushed away by the nozzle. The matrix materials could be sandwiched between the printed filaments. Sparrman et al.[26] reported that by decreasing the stepover distance in *Z*-axis, the fusion of printed lines and air-tightness can be improved. Figure 2c,d shows three cylindrical tubes printed by inks with different storage moduli. The ink is prepared by mixing different ratios of DOW 1700 and Sylgard 184 in weight ratios of 7:3, 5:5, and 3:7. Printed in different stepover distance, all of the three structures are air-tight. However, as the concentration of DOW 1700 decreases, the storage modulus of the ink lowers (Figure S2, Supporting Information) and the printing quality of the tube is worse. The mismatch between the stepover distance and line height result in wrinkles on the printed surface (Figure 2d). Therefore, we modify the rheological property of the inks to increase the storage moduli for successful printing. As shown in Figure 2e, the moduli of the PDMS inks are one or two orders of magnitude higher than the matrix.[5] All three inks are shear thinning and they are suitable for 3D printing (Figure S3, Supporting Information).

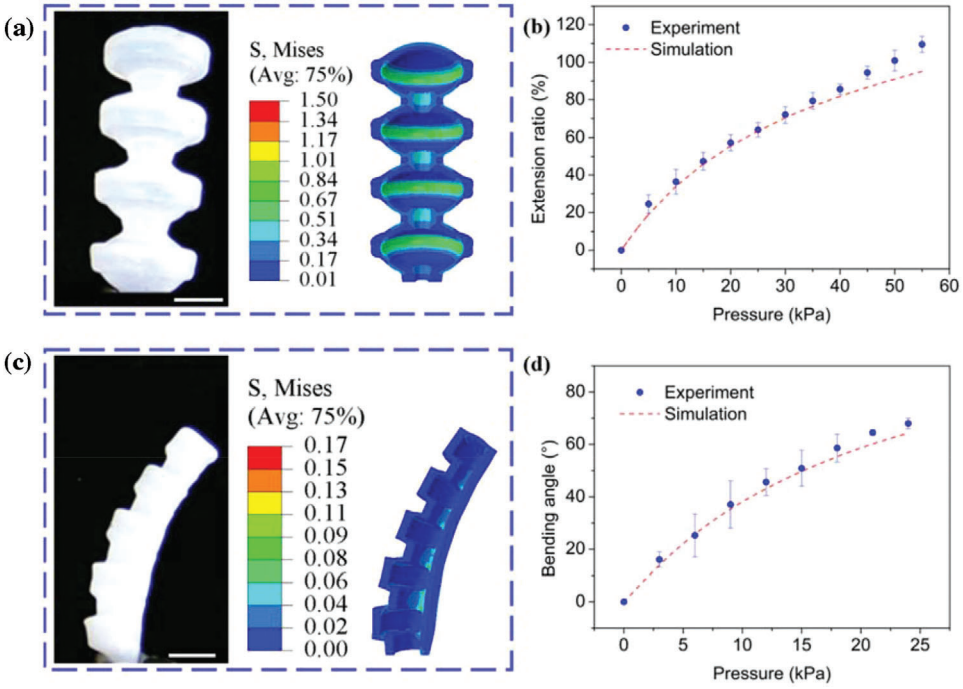

Figure 3. Performance of pneumatic actuators: a) Experimentally measured (left) and simulated (right) elongation of the linear actuator with an inflating pressure of ≈50 kPa (scale bar: 1 cm); b) Relationship between experiment and simulation elongation ratios and inflating pressure; c) Experimentally measured (left) and simulated (right) bending of the bending actuator with the inflating pressure of ≈12 kPa (scale bar: 1 cm); d) Relationship between bending angles and inflating pressures showing both experiment and simulation results.

The multi-material printing provides a versatile digital manufacturing platform to integrate materials having very different mechanical properties. In our work, we select three different silicone-based inks with elastic moduli of ≈1000, ≈500, and ≈200 kPa. Their maximum strains are ≈107%, ≈350%, and ≈900%, respectively (Figure 2f). The formulations of the inks are listed in materials and method section. The Ogden 1st model is used to describe the hyperplasticity of the hard ($\mu = 0.35$ MPa, $\alpha = 2.802$), intermediate ($\mu = 0.26$ MPa, $\alpha = 2.14$), and soft inks ($\mu = 0.14$ MPa, $\alpha = 2.30$). The correlation coefficients of the fitting are all larger than 0.99 (Figure S4, Supporting Information). The adhesion between the different materials is tested by uniaxial tensile measurement of the dogbone-shaped samples consisted of two materials. The sample breaks within the low tensile stress section (hard < intermediate < soft) instead of at the interfaces between the two materials, which proves the good adhesion between our printed materials (Figure S5, Supporting Information).

3.2. Performance of the Printed Pneumatic Actuator

In our work, we first print different actuators and simulate their motions using Abaqus. The simulation settings are listed in material and methods section. The FEA model provides a good quantitative prediction of the experimental data, which can guide the design before fabrication.

The linear actuator is first printed using the intermediate ink and evaluated on the platform consisting of several syringe pumps, pressure gauges, and cameras. The elongation is recorded by the camera and calculated using MATLAB R2020a (MathWorks Inc.). The bellow-based shape allows the linear motion, which is proved by the experiment and simulation (**Figure 3**a). The actuator extends as the pressure increases (Figure 3b). The elongation ratio reaches ≈109% at a pressure of ≈55 kPa. (Video S2: Supporting Information). The PneuNet-based[8] bending actuator is then printed using soft ink and its bending performance is evaluated. The bending motion is generated due to the asymmetry of the structure (Figure 3c). The bending angle increases accordingly as the pressure increases. When the pressure increases to ≈24 kPa, the bending angle reaches ≈68° (Figure 3d). However, the radial ballooning is obvious, and the constrained layer of the actuator in Figure 3c also expends outward. Therefore, the bending angle is limited (Video S2: Supporting Information).

To solve the ballooning effect,[30] the intermediate (red) and hard (blue) inks are used to print the bending actuators. The hard ink functions as the constrained layer. The actuator will bend toward the constrained layer when inflated (**Figure 4**a). Comparing to the performance of the actuator printed by a single material, the bend angle and working pressure are improved greatly from ≈24 kPa and ≈68° to ≈121° and ≈80 kPa, respectively (Figure 4b). At the same time, the ballooning effect is eliminated apparently (Video S3: Supporting Information). The simulation results provide a good quantitative prediction of the motion, despite that the simulations are larger than the experimental ones at the higher pressure. The disagreements may come from material testing limited to uniaxial tension. Improved accuracy might be possible by performing multiaxial material testing.[21]

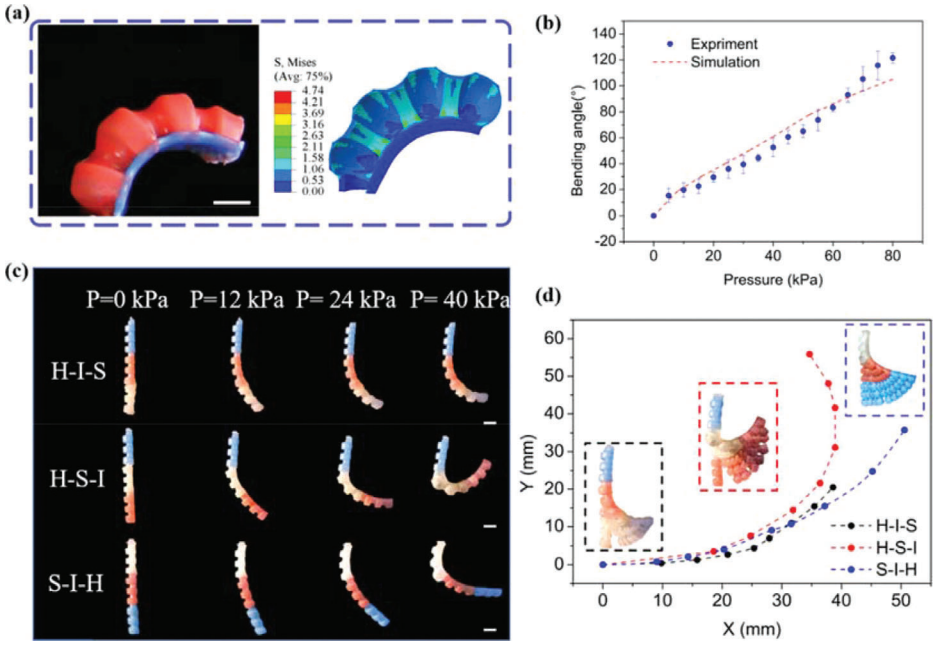

Figure 4. Multi-material 3D printing of soft actuators: a) Actuator bending with inflating pressure of 80 kPa (scale bar: 1 cm, left: experiment; right: simulation); b) Relationship between bending angles and inflating pressures c) Three inks with different stiffness are used to print bending actuators (scale bar: 2 cm), which is noted by H-I-S, H-S-I, and S-I-H. d) The tip point trajectories of three actuators.

To further demonstrate the ability of multi-material printing, three different bending actuators connected in series are printed altogether by MJDIW. In our design, each segment has the dimension of ≈15 mm in length, ≈8 mm in width and ≈27 mm in height. The wall thickness is controlled to be constant by adjusting the printing pressure even when using different inks (Figure S9, Supporting Information). Under the same driving pressure, the segment in soft material bends the largest while the hard one hardly bends. By changing the printing order of segments printed by different materials (white for soft ink, red for intermediate ink, and blue for hard ink), various bending curvatures can be obtained under the same pressure (Figure 4c). Different trajectories of the end points can also be obtained (Figure 4d, Video S4: Supporting Information). Also, we simulate the motion of the actuators fabricated by three materials, and the results are shown in Figure S10 (Supporting Information). The FEA can predict the motion of multi-material actuator well at low pressures. But there is slight difference at high pressure. The disagreements may because of the complex mechanical property of the junction of different materials, which is simplified in our simulation.

3.3. Application of a Soft Printed Pneumatic Manipulator

For our last demonstration, a soft pneumatic manipulator is printed to demonstrate the multimaterial and monolithic printing ability of complex soft robots. The manipulator consists of a soft arm and a soft gripper, which are printed using hard and intermediate inks, respectively. (Figure 1b). The soft arm is printed using three parallel elongation actuators with the diameter of ≈14 mm and length of ≈40 mm. The gripper is composed of three bending actuators with the length of ≈25 mm. Three elongation actuators are controlled by three individual air supplies. The air chambers of three bending actuators are connected together with one air supply. Coordinating all three elongation actuators, the arm is able to reach different positions (Video S5: Supporting Information). To evaluate the performance of manipulator, a custom-made control system is built (Figure S11, Supporting Information). We use three pumps which are controlled by a micro-computing unit to inflate and deflate the elongation actuators. The corresponding relationship and the coordinate system are shown in **Figure 5a**. Three pumps work alternately to drive the manipulator to follow a circular trajectory. The whole process can be divided into eight parts. Each part lasts for 5 s, and the status of three pumps (1 for inflating, 0 for closing and −1 for deflating) are shown in Figure 5b. The pressures of three actuators are also recorded (Figure 5b). When the actuator is inflated, the pressure increases from 0 to ≈30 kPa. We use two cameras to catch the end of the soft manipulator (Video S6: Supporting Information), and the results are shown in Figure 5c. From $t = 0$ to $t = 40$ s, the trajectory of the manipulator in XY plane is an approximate circle with the diameter of ≈50 mm, and an arc in YZ plane. Figure 5d shows the state of the manipulator at the time of 0, 5, 10, 20, and 25 s. Objects with different weights (pen, cube, litchi, with the weight of ≈20 to ≈50 g) can be grasped under the different driving pressure (Figure 5e). To further study the grasp ability, we drive the soft manipulator to grasp the weights from ≈10 to ≈100 g through 3D printed hooks (Figure S12, Supporting Information). As the mass increases, the grasping pressure also increases (Figure S13, Supporting Information). The gripper weight is ≈9 g in total and it can grasp the weight of ≈100 g under the driving pressure of ≈120.6 kPa. At last, we control the soft manipulator to finish a shaft and hole mating task with the cooperation of a 3-axies CNC motion platform (Figure 5f, Video S7:

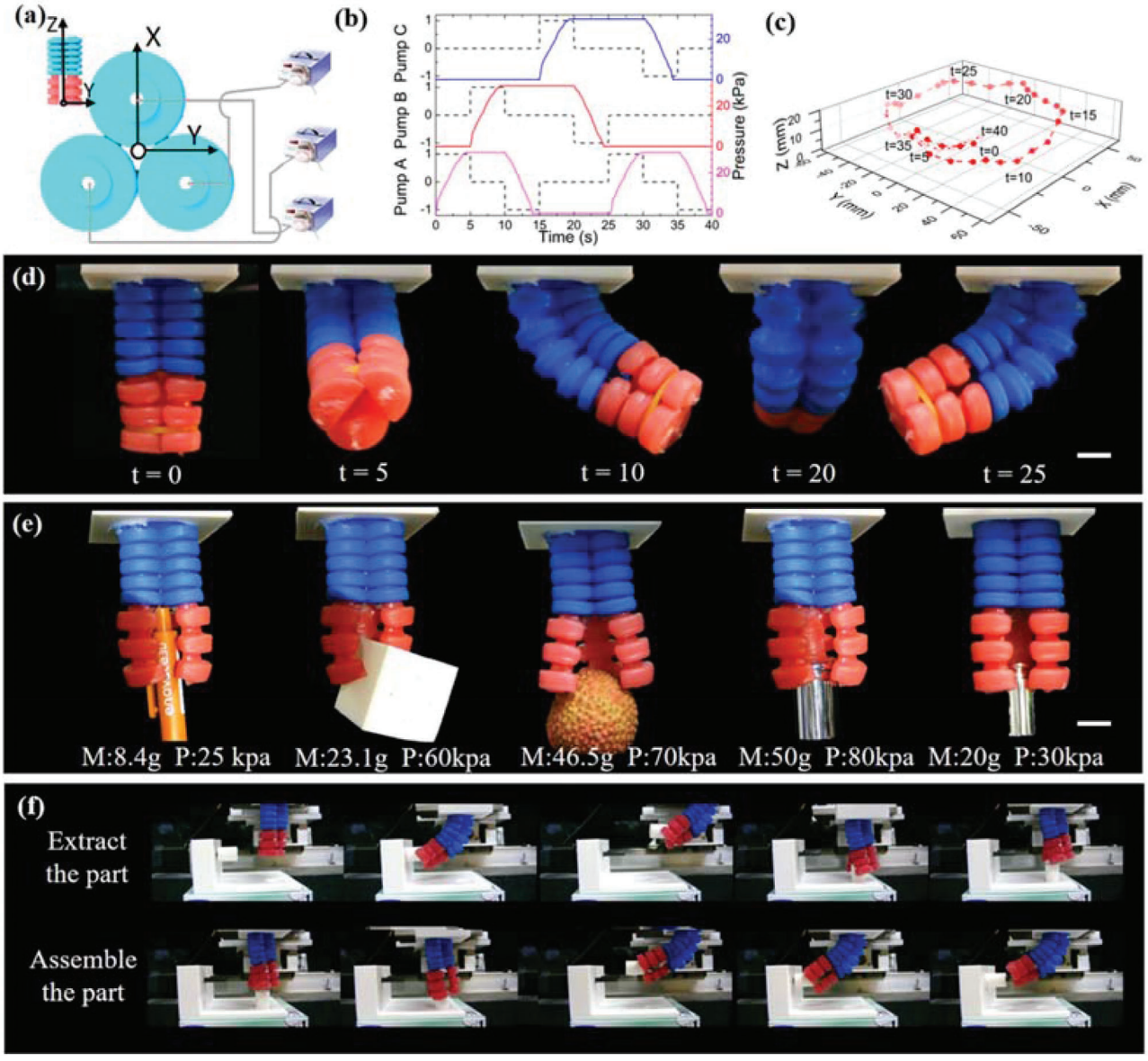

Figure 5. Demonstration of the printed soft pneumatic manipulator: a) The arm of the manipulator is controlled by three independent pumps. The coordinate system is also shown in the figure. b) The whole process can be divided into eight parts, with each part lasts for 5 s. The states of the three pumps: 1 for inflating, 0 for closing and −1 for deflating. The pressure is also recorded by pressure gauges. c) The trajectory of the end point controlled by the method in (b). From $t = 0$ to $t = 40$ s, it follows a circle trajectory in its workspace. d) The state of the manipulator at the time of 0, 5, 10, 20, and 25 s. e) The gripper can grasp different objects under different driving pressure. f) Printed manipulator can finish the shaft and hole mating task. Top: the manipulator bends 90° to extract the part from the shaft. Bottom: the manipulator inserts the part into the shaft.

Supporting Information). The manipulator bends ≈90° to grasp the part inserted on the shaft, extracts it and finally places it on the plane vertical to the axis of the shaft. Then the manipulator successfully picks up the part from the plane and inserts it into the shaft.

3.4. Future Work

The nozzle utilized in our work has an inner diameter of ≈650 µm. Custom-made glass microcapillary with inner diameters of ≈100 µm is also used to print smaller actuators with higher resolution (Figure S14, Supporting Information). The inner channel can be seen through the transparent materials. Although the smallest size is limited by the interfacial tensions of the ink and matrix,[31] the actuators at the micrometer scale can still be printed. Therefore, this method has the potential to fabricate micrometer scale pneumatic soft robots in high resolution. The larger size of the structure (≈1 m scale) can also be printed by this method, and it only needs larger motion platform, larger matrix tank and the ink reservoirs which can supply large quantity of materials.

The integration of soft sensors with soft actuators has been a spotlight. Ryan et al. used embedded 3D printing to print curvature, touch, and temperature sensors into soft fingers.[5] However, the external shape of soft actuators is limited by the mold structure. Here, our proposed method enables the freeform 3D printing of complex pneumatic structures. Future work employing dual embedded 3D printing method is underway to monolithically integrate the soft actuators and sensors.

4. Conclusions

In this work, we report a MJDIW method to fabricate soft pneumatic actuators and robots. Experimental results show that our method is a promising method to print the soft robots with complex structures while integrating multiple materials having distinct mechanical properties (Table S3, Supporting Information). To explore the printing parameters, rheological properties and printing parameters are systematically investigated. To demonstrate the freeform printing ability, elongation and bending actuators are printed. Their performances are evaluated by simulations and experiments. The successful printing of a soft manipular with a soft arm and a gripper illustrates the ability of monolithic printing of complex structures featuring different materials. The printed manipulator can follow the desired trajectory under the control of a custom-made control unit. The mating task shows that our printed soft pneumatic robots are capable of completing delicate biomimetic tasks.

Supporting Information

Supporting Information is available from the Wiley Online Library or from the author.

Acknowledgements

This work was supported by Zhejiang Key R&D Program No.2021C03157, the "Construction of a Leading Innovation Team" project by the Hangzhou Municipal government.

Conflict of Interest

The authors declare no conflict of interest.

Data Availability Statement

The data that support the findings of this study are available from the corresponding author upon reasonable request.

Keywords

additive manufacturing, embedded direct ink writing, multi-material 3D printing, soft robots

Received: October 28, 2021
Revised: January 28, 2022
Published online: February 14, 2022

[1] J. Shintake, V. Cacucciolo, D. Floreano, H. Shea, *Adv. Mater.* **2018**, *30*, 1707035.
[2] a) K. C. Galloway, K. P. Becker, B. Phillips, J. Kirby, S. Licht, D. Tchernov, R. J. Wood, D. F. Gruber, *Soft Robot.* **2016**, *3*, 23; b) B. T. Phillips, K. P. Becker, S. Kurumaya, K. C. Galloway, G. Whittredge, D. M. Vogt, C. B. Teeple, M. H. Rosen, V. A. Pieribone, D. F. Gruber, *Sci. Rep.* **2018**, *8*; c) N. R. Sinatra, C. B. Teeple, D. M. Vogt, K. K. Parker, D. F. Gruber, R. J. Wood, *Sci. Robot.* **2019**, *4*, eaax5425.
[3] a) T. Ranzani, G. Gerboni, M. Cianchetti, A. Menciassi, *Bioinspir. Biomim.* **2015**, *10*, 035008; b) M. Runciman, A. Darzi, G. P. Mylonas, *Soft Robot.* **2019**, *6*, 423.
[4] F. Connolly, P. Polygerinos, C. J. Walsh, K. Bertoldi, *Soft Robot.* **2015**, *2*, 26.
[5] R. L. Truby, M. Wehner, A. K. Grosskopf, D. M. Vogt, S. G. M. Uzel, R. J. Wood, J. A. Lewis, *Adv. Mater.* **2018**, *30*, 1706383.
[6] a) K. Song, S. H. Kim, S. Jin, S. Kim, S. Lee, J. - S. Kim, J. - M. Park, Y. Cha, *Sci. Rep.* **2019**, *9*, 1; b) K. Elgeneidy, N. Lohse, M. Jackson, *Mechatronics* **2018**, *50*, 234.
[7] A. K. Mishra, T. J. Wallin, W. Pan, P. Xu, K. Wang, E. P. Giannelis, B. Mazzolai, R. F. Shepherd, *Sci. Robot.* **2020**, 5, eaaz3918.
[8] H. Kim, J. Choi, K. K. Kim, P. Won, S. Hong, S. H. Ko, *Nat. Commun.* **2021**, *12*, 1.
[9] A. D. Marchese, R. K. Katzschmann, D. Rus, *Soft Robot* **2015**, *2*, 7.
[10] H. Zhao, Y. Li, A. Elsamadisi, R. Shepherd, *Extreme Mech. Lett.* **2015**, *3*, 89.
[11] B. Mosadegh, P. Polygerinos, C. Keplinger, S. Wennstedt, R. F. Shepherd, U. Gupta, J. Shim, K. Bertoldi, C. J. Walsh, G. M. Whitesides, *Adv. Funct. Mater.* **2014**, *24*, 2163.
[12] O. D. Yirmibesoglu, J. Morrow, S. Walker, W. Gosrich, R. Cañizares, H. Kim, U. Daalkhaijav, C. Fleming, C. Branyan, Y. Menguc, *2018 IEEE Int. Conf. on Soft Robotics*, IEEE, Piscataway, NJ **2018**.
[13] a) W. Hu, G. Alici, *Soft Robot.* **2020**, *7*, 267; b) C. Tawk, M. in het Panhuis, G. M. Spinks, G. Alici, *Soft Robot.* **2018**, *5*, 685; c) H. K. Yap, H. Y. Ng, C.-H. Yeow, *Soft Robot.* **2016**, *3*, 144.
[14] B. N. Peele, T. J. Wallin, H. Zhao, R. F. Shepherd, *Bioinspir. Biomim.* **2015**, *10*, 055003.
[15] D. K. Patel, A. H. Sakhaei, M. Layani, B. Zhang, Q.i Ge, S. Magdassi, *Adv. Mater.* **2017**, *29*, 1606000.
[16] R. B. Scharff, E. L. Doubrovski, W. A. Poelman, P. P. Jonker, C. C. Wang, J. M. Geraedts, in *Soft Robotics: Trends, Applications and Challenges*, Springer, New York **2017**, p. 23.
[17] D. Rus, M. T. Tolley, *Nature* **2015**, *521*, 467.
[18] J. D. Hubbard, R. Acevedo, K. M. Edwards, A. T. Alsharhan, Z. Wen, J. Landry, K. Wang, S. Schaffer, R. D. Sochol, *Sci. Adv.* **2021**, *7*, eabe5257.
[19] J. Plott, A. Shih, *Addit. Manuf.* **2017**, *17*, 1.
[20] T. E. Greenwood, S. E. Hatch, M. B. Colton, S. L. Thomson, *Addit. Manuf.* **2021**, *37*, 101681.
[21] M. Schaffner, J. A. Faber, L. Pianegonda, P. A. Rühs, F. Coulter, A. R. Studart, *Nat. Commun.* **2018**, *9*, 878.
[22] T. Bhattacharjee, S. M. Zehnder, K. G. Rowe, S. Jain, R. M. Nixon, W. G. Sawyer, T. E. Angelini, *Sci. Adv.* **2015**, *1*, 1500655.
[23] C. S. O'Bryan, T. Bhattacharjee, S. Hart, C. P. Kabb, K. D. Schulze, I. Chilakala, B. S. Sumerlin, W. G. Sawyer, T. E. Angelini, *Sci. Adv.* **2017**, *3*, 1602800.
[24] T. J. Hinton, A. Hudson, K. Pusch, A. Lee, A. W. Feinberg, *ACS Biomater. Sci. Eng.* **2016**, *2*, 1781.
[25] K. Hajash, B. E. Sparrman, C. Guberan, J. S. Laucks, S. Tibbits, *3D Print. Addit. Manuf.* **2017**, *4*, 123.
[26] B. Sparrman, C. du Pasquier, C. Thomsen, S. Darbari, R. Rustom, J. Laucks, K. Shea, S. Tibbits, *Addit. Manuf.* **2021**, *40*, 101860.
[27] X. Ke, J. Jang, Z. Chai, H. Yong, J. Zhu, H. Chen, C. F. Guo, H. Ding, Z. Wu, *Soft Robot.* **2021**. https://doi.org/10.1089/soro.2020.0207

[28] Z. Gong, X. Fang, X. Chen, J. Cheng, Z. Xie, J. Liu, B. Chen, H. Yang, S. Kong, Y. Hao, T. Wang, J. Yu, L.i Wen, *Int. J. Robot. Res.* **2021**, *40*, 449.
[29] A. K. Grosskopf, R. L. Truby, H. Kim, A. Perazzo, J. A. Lewis, H. A. Stone, *ACS Appl. Mater. Interfaces* **2018**, *10*, 23353.
[30] Y. Elsayed, A. Vincensi, C. Lekakou, T. Geng, C. M. Saaj, T. Ranzani, M. Cianchetti, A. Menciassi, *Soft Robot.* **2014**, *1*, 255.
[31] C. S. O'bryan, T. Bhattacharjee, S. R. Niemi, S. Balachandar, N. Baldwin, S. T. Ellison, C. R. Taylor, W. G. Sawyer, T. E. Angelini, *MRS Bull.* **2017**, *42*, 571.